Int. J. Heat Mass Transfer. Vol. 24, No. 8, pp. 1421–1430, 1981.
Printed in Great Britain

0017-9310/81/081421-10 $02.00/0
Pergamon Press Ltd.

COMBINED CONDUCTION, CONVECTION, GAS RADIATION AND PARTICLES RADIATION IN MHD DIFFUSERS

R. K. AHLUWALIA and K. H. IM
Argonne National Laboratory, 9700 South Cass Avenue, Argonne, IL 60439, U.S.A.

(*Received* 23 *September and in revised form* 27 *February* 1981)

Abstract—Heat transfer in MHD diffusers, by conduction, convection, gas radiation, and slag particles radiation, is analyzed by simultaneously solving the radiation transport equation and a set of quasi-three-dimensional gasdynamic equations. Carbon dioxide, water vapor, and potassium atoms are considered to be the principal gases participating in gas radiation. The non-grey radiation transport equation is solved by invoking the P_1 approximation. The absorption coefficients for CO_2 and H_2O are evaluated from the exponential wide-band model and for K atoms from certain correlations. The efficiency factors for extinction and scattering by particles are calculated from Mie theory. For a reference diffuser geometry appropriate for a 1700 MW thermal MHD plant, the heat transfer by convection is found to be 25 MW, and the radiative heat transfer varies from 44 to 79 MW, depending on the rate of ash carryover into the channel. Results reveal that the heat transfer is sensitive to the ash carryover into the channel, slag particle size spectrum, electrical conductivity of ash, gas composition, and wall emissivity. It is observed that, because of multiple scattering, the particles shield the short wavelength radiation emitted by potassium atoms.

NOMENCLATURE

A,	cross-sectional area;
a_ν, b_ν,	parameters defined in equations (13) and (17);
a_l, b_l,	Mie complex scattering coefficients;
C_p,	pressure recovery coefficient;
h,	enthalpy;
I_ν,	radiation intensity;
$I_{b\nu}$,	Planck function at gas temperature;
$I_{w\nu}$,	Planck function at wall temperature;
G_ν,	incident radiation;
m,	complex refractive index;
n, N,	particle-size distribution function and number density;
$N_0, \langle r\rangle_0$,	number density and average size at diffuser inlet;
p,	pressure;
$\dot{q}_r$,	radiative heat flux;
r,	particle radius;
S_ν,	scattering function;
u,	axial component of gas velocity;
v,	normal component of gas velocity;
W,	diffuser width;
x, y, z,	Cartesian coordinates.

Greek symbols

α_ν,	parameter defined in equation (21);
β_ν, ω_ν,	extinction coefficient and scattering albedo;
τ, τ_0,	optical thickness and its value at wall;
τ_{xy}, τ_s,	shear stress and its value at wall;
ρ,	gas density;
μ_{eff},	effective viscosity;
μ,	cosine of the cone angle;
ε_w,	wall emissivity;
$\delta_1, \delta_2, \delta_3$,	displacement, momentum and enthalpy thickness;
δ,	boundary layer thickness;
$\chi_{e\nu}, \chi_{s\nu}$,	efficiency factors for extinction and scattering;
λ,	wavelength;
θ,	divergence half angle of diffuser;
σ_e,	electrical conductivity of slag [S m^{-1}].

Subscripts

c,	centerline;
w, s,	wall;
ν,	spectral;
$\langle\ \rangle$,	average.

INTRODUCTION

IN THE open-cycle magnetohydrodynamic (MHD) method of energy conversion, air and fuel mixture is combusted at a temperature of 2700 K or higher, and seeded with potassium to render the combustion products electrically-conducting. The combustion gas is accelerated to a high velocity in a nozzle, and passed through the MHD channel where a magnetic field is applied in a direction normal to the flow thereby effecting a direct conversion of thermal and kinetic energy of the combustion gas to electricity. The spent gas exiting the channel still has a significant amount of thermal and kinetic energy and must be slowed in a diffuser to allow further processing and to recover some of the dynamic pressure [1]. The purpose of this work is to analyze heat transfer in MHD diffusers of coal-fired plants.

There are three distinguishing characteristics of the flow entering an MHD diffuser. First, the flow has

thick boundary layers with an inlet blockage higher than 10% [2]. Second, the gas temperature is high enough (about 2300 K) for radiation to be a significant mode of heat transfer. The third characteristic relates to the presence of potassium atoms and slag particles in the combustion gas. The source of potassium atoms is the seed that was added in the combustor for the enhancement of electrical conductivity. The potassium atoms do participate in promoting gas radiation [3]. The nature and source of slag particles is more complex and is explained in the following paragraph.

The high temperature prevailing in the coal-fired MHD combustor causes a substantial amount of coal ash to vaporize. The vaporized ash and some of the unvaporized ash particles flow into the MHD channel. As the gas cools down in the MHD channel from the combined effects of power extraction and heat loss, the supersaturation ratio of ash vapor rises; the supersaturation ratio is defined as the partial pressure of a gaseous constituent normalized by the saturation pressure. At some point, the supersaturation ratio attains the critical value at which the ash vapors condense out in the form of liquid droplets (slag particles) by the process of homogeneous nucleation. Paralleling the homogeneous nucleation process of slag vapor removal is the direct condensation (heterogeneous nucleation) of ash vapor on the slag particles already present. The final size distribution of slag particles evolves as the homogeneous nucleation and heterogeneous nucleation mechanisms compete to strip the gas of slag vapor; the former mechanism forms new particles, whereas the latter tends to restrict the population growth by condensing vapor on the particles. For more comprehensive details see [2] and [3]. For the channel operating conditions of [2], all the ash vapors had condensed out before the gas reached the channel exit.

The nucleated slag particles are submicrometer in size and numerous in number (10^7–10^9/cm^3). The coal slag is electrically conducting and absorbs as well as scatters thermal radiation. It was found in this study that in the diffuser the radiant heat transfer attributable to slag particles and seed may exceed that by gas alone by a factor of two or even three. Besides potassium atoms and slag particles, other species participating in radiation are carbon dioxide and water vapor.

In the past, Doss [4] and Roy [5] have analyzed the performance of MHD diffusers with high blockages. Neither of the two studies included the sizeable contributions of gas and particle radiation to heat transfer. This work serves to remove this limitation in the formulations of [4] and [5] by solving a set of quasi-three-dimensional gasdynamic equations in conjunction with the radiation transport equation. The possibility of radiation scattering by slag particles is included in the radiation transport equation. The efficiency factors for extinction and scattering (caused by particles) are evaluated directly from Mie theory [6]. The absorption coefficients for carbon dioxide and water vapor are computed from the exponential wide band model [7], and for potassium atoms from certain correlations of experimental data [2]. A closed-form solution of the radiation transport equation is first obtained by invoking the P_1 approximation [8]. The complete diffuser model equations are then solved numerically.

Various diffuser calculations are performed for diffuser entrance conditions consistent with the channel exit conditions of [2]. The slag particle size spectra enumerated in [2] are employed in the form of histograms in these calculations. Although the model is applied to the flow situation in MHD diffusers only, the combined conduction, convection, gas radiation and particulate radiation model formulated in this paper and its analysis is sufficiently general to be applied to many situations in which the three modes of heat transfer are equally important. Typical applications where the model may be useful include combustion chambers, whether coal, gas, or oil-fired, and thermal shields for space re-entry vehicles.

DIFFUSER MODEL AND ANALYSIS

The governing equations are comprised of quasi-three-dimensional gasdynamic equations, an equation to ensure slag particles number conservation, and a radiation transport equation. The particle number conservation equation is linked to gasdynamics through the average flow velocity. The radiation transport equation supplies the divergence of radiant heat flux and wall heat flux to the energy equation, but is itself coupled to gasdynamics through the temperature field. The gasdynamic equations listed below are these derived in [9]. Briefly, the approach consists of partially integrating the gasdynamic equations in the sidewall direction. In so doing, the sidewall effects become manifest through the displacement thicknesses characterizing the flux deficit because of sidewall boundary layers, i.e. displacement thickness for mass deficit, momentum thickness for momentum deficit, and enthalpy thickness for energy deficit. Explicit terms also appear to account for friction and heat transfer on the sidewalls. The principal advantage of this approach is that it permits a fully 3-D flow to be analyzed by a set of two-dimensional equations.

Continuity

$$\frac{\partial}{\partial x}[\rho u(W - 2\delta_{1s})] + \frac{\partial}{\partial y}[\rho v(W - 2\delta_{1s})] = 0. \quad (1)$$

x-*Momentum*

$$\frac{\partial}{\partial x}[\rho uu(W - 2\delta_{2s})] + \frac{\partial}{\partial y}[\rho uv(W - 2\delta_{2s})] = -W\frac{\partial p}{\partial x} + W\frac{\partial}{\partial y}\left(\mu_{\text{eff}}\frac{\partial u}{\partial y}\right) - 2\tau_s. \quad (2)$$

y-*Momentum*

$$\frac{\partial p}{\partial y} = 0. \quad (3)$$

Total energy

$$\frac{\partial}{\partial x}[\rho u(h+\tfrac{1}{2}u^2)(W-2\delta_{3s})] + \frac{\partial}{\partial y}[\rho v(h+\tfrac{1}{2}u^2)(W-2\delta_{3s})] = W\frac{\partial}{\partial y}\left(k_{\text{eff}}\frac{\partial T}{\partial y}\right) - W\frac{\partial \dot{q}_r}{\partial y} + W\frac{\partial}{\partial y}(u\tau_{xy}) - 2(\dot{q}_c+\dot{q}_{rs}) \quad (4)$$

where δ_{1s}, δ_{2s}, and δ_{3s} are, the displacement, momentum, and enthalpy thicknesses of the sidewall boundary layers, respectively [9].

Slag number conservation

$$\frac{\mathrm{d}}{\mathrm{d}x}(NA\langle u\rangle) = 0. \quad (5)$$

Radiation transport equation

$$\mu\frac{\partial I_\nu}{\partial y} + \beta_\nu I_\nu(y,\mu) = (1-\omega_\nu)\beta_\nu I_{b\nu} + \frac{1}{2}\omega_\nu\beta_\nu\int_{-1}^{1} S_\nu(\mu,\mu')I_\nu(y,\mu')\,\mathrm{d}\mu'. \quad (6)$$

The foregoing set of equations essentially describes a two-dimensional development of flow, with certain correction terms included to account for the displacement effects of the sidewall boundary layers. In the spirit of parabolic flow analysis, diffusion of heat and momentum in the flow direction has been neglected in these equations in comparison to diffusion in transverse direction. Further assumptions implicit in equations (1)–(6) and those made in the course of the analysis are the following:

(1) The electrode and sidewall boundary layers are similar to each other, thus implying that δ_{1s}, δ_{2s}, δ_{3s}, and friction and heat transfer on the sidewalls are equal to their counterparts on the electrode walls.

(2) Slag particles are in velocity and thermal equilibrium with the gas—a justifiable assumption considering that the characteristic relaxation time of submicron particles is of the order of microseconds.

(3) Slag vapors have completely condensed out in the channels so that no further nucleation can occur in the diffuser. This assumption is supported by analytical results presented in [2].

(4) On the basis of order of magnitude type estimates, any changes in total number density of particles due to agglomeration or due to slag deposition on diffuser walls have been neglected.

Analytical solution of radiation transport equation

The gradient of radiant heat flux can be obtained by integrating (6) with respect to μ and ν

$$\frac{\mathrm{d}\dot{q}_r}{\mathrm{d}y} = 4\pi\int_0^\infty (1-\omega_\nu)\beta_\nu\left(I_{b_\nu} - \frac{G_\nu}{4\pi}\right)\mathrm{d}\nu \quad (7)$$

where G_ν, the incident radiation, may be evaluated by integrating the spectral radiation intensity (I_ν) as

$$G_\nu(y) = 2\pi\int_{-1}^{1} I_\nu(y,\mu)\,\mathrm{d}\mu \quad (8)$$

and

$$\dot{q}_r = 2\pi\int_0^\infty \mathrm{d}\nu\int_{-1}^{1}\mu I_\nu(y,\mu)\,\mathrm{d}\mu.$$

Equation (7) in spectral form is

$$\frac{\mathrm{d}\dot{q}_{r\nu}}{\mathrm{d}\tau} + (1-\omega_\nu)G_\nu = 4\pi(1-\omega_\nu)I_{b\nu} \quad (9)$$

where τ is the optical thickness, defined as

$$\tau = \int_0^y \beta_\nu(y')\,\mathrm{d}y'.$$

In order to solve equation (6) for G_ν, expand I_ν and S_ν in series of Legendre polynomials. Retaining only the zero- and first-order terms in these series and performing the operations indicated in P_1 approximation [8], one has

$$I_\nu(\tau,\mu) = \frac{1}{4\pi}G_\nu(\tau) + \frac{3}{4\pi}\dot{q}_{r\nu}(\tau)\mu \quad (10)$$

$$\frac{\mathrm{d}G_\nu}{\mathrm{d}\tau} + 3\dot{q}_{r\nu} = 0. \quad (11)$$

In writing equation (11), a nonessential assumption has been made, namely, the scattering function is an isotropic one. Equations (9) and (11) may be combined to produce a single equation for G_ν.

$$\frac{\mathrm{d}^2G_\nu}{\mathrm{d}\tau^2} - a_\nu^2 G_\nu = -4\pi a_\nu^2 I_{b\nu} \quad (12)$$

where

$$a_\nu = \sqrt{[3(1-\omega_\nu)]}. \quad (13)$$

The centerline symmetry condition and the boundary condition for specularly reflecting walls are

$$I_\nu(0,-\mu) = I_\nu(0,\mu) \quad \mu>0 \quad (14)$$

$$I_\nu(\tau_0,-\mu) = \varepsilon_w I_{w\nu} + (1-\varepsilon_w)I_\nu(\tau_0,\mu) \quad \mu>0. \quad (15)$$

Using Mark's boundary condition [10], μ in equation (11) is replaced by $\mu_0(\equiv 1/\sqrt{3})$. This is the value of μ that makes the second-order solution identically equal to zero. Using equation (11), the two boundary conditions can be rewritten as

$$\left(\frac{\mathrm{d}G_\nu}{\mathrm{d}\tau}\right)_0 = 0$$

and

$$G_\nu(\tau_0) + b_\nu\left(\frac{\mathrm{d}G_\nu}{\mathrm{d}\tau}\right)_{\tau_0} = 4\pi I_{w\nu} \quad (16)$$

where

$$b_\nu = \frac{1}{\sqrt{3}}\left(\frac{2-\varepsilon_w}{\varepsilon_w}\right). \quad (17)$$

Using the Green function approach and assuming a_ν to

be a slowly varying function, the following solution for G_ν may be constructed

$$G_\nu = 4\pi I_{w\nu} + 4\pi \int_0^{\tau_0} K_\nu(\tau|\xi) a_\nu^2 (I_{b\nu} - I_{w\nu})\, d\xi \quad (18)$$

with

$$K_\nu(\tau|\xi) = \frac{[\exp(a_\nu\xi) + \exp(-a_\nu\xi)]}{2(1-\alpha_\nu)a_\nu} \times [\alpha_\nu \exp(a_\nu\tau) + \exp(-a_\nu\tau)] \quad \tau > \xi \quad (19)$$

$$K_\nu(\tau|\xi) = \frac{[\alpha_\nu \exp(a_\nu\xi) + \exp(-a_\nu\xi)]}{2(1-\alpha_\nu)a_\nu} \times [\exp(a_\nu\tau) + \exp(-a_\nu\tau)] \quad \tau < \xi \quad (20)$$

where

$$\alpha_\nu = \frac{b_\nu a_\nu - 1}{b_\nu a_\nu + 1} \exp(-2a_\nu\tau_0). \quad (21)$$

This completes the solution.

Radiation properties

Carbon dioxide, water vapor, and potassium atoms are considered to be the principal participating gases. The spectral absorption coefficients for carbon dioxide and water vapor are evaluated from the exponential wideband model [7]. For atomic potassium, effective absorption for potassium occurs in the range $746 < \lambda(\mu m) < 820$ and is given by the correlations presented in [2].

Mie theory [6] is employed to calculate the scattering and absorption coefficients for slag particles. Without going into lengthy details, the following are the efficiency factors for extinction and scattering

$$\chi_{e\nu} = 2\left(\frac{\lambda}{2\pi r}\right)^2 \sum_{l=0}^{\infty} (2l+1)\,\mathrm{Re}\,(a_l + b_l) \quad (22)$$

$$\chi_{s\nu} = 2\left(\frac{\lambda}{2\pi r}\right)^2 \sum_{l=0}^{\infty} (2l+1)(|a_l|^2 + |b_l|^2) \quad (23)$$

where the coefficients, a_l and b_l, are complex numbers. These coefficients are functions of two parameters, $2\pi r/\lambda$ and m, the complex refractive index.

For a medium containing particles of many sizes, the overall extinction coefficient, gas-plus-particles, and scattering albedo are determined by the following equations

$$\beta_\nu = \kappa_\nu^g + \pi \int_0^\infty \chi_{e\nu}(m, 2\pi r/\lambda) n(r) r^2\, dr$$

$$\omega_\nu = \frac{1}{\beta_\nu}\left[\pi \int_0^\infty \chi_{s\nu}(m, 2\pi r/\lambda) n(r) r^2\, dr\right].$$

Finally, the particle spectrum is input to the computer program in the form of histograms so that the equations for β_ν and ω_ν are numerically evaluated as follows:

$$\beta_\nu = \kappa_\nu^g + \pi \sum_i \chi_{e\nu}(m, 2\pi r_i/\lambda) \bar{N}_i \bar{r}_i^2 \quad (24)$$

and

$$\omega_\nu = \frac{1}{\beta_\nu}\left[\pi \sum_i \chi_{s\nu}(m, 2\pi r_i/\lambda) \bar{N}_i \bar{r}_i^2\right] \quad (25)$$

where κ_ν^g is the absorption coefficient of the gas.

Turbulent model

The two-layer eddy diffusivity model of Cebeci and Smith [11] is used in the present analysis. Effects of wall roughness on fluid flow are simulated by displacing the coordinate in the inner region, as suggested by Cebeci and Chang [12]. Effects of wall roughness on heat transfer are represented by adopting the effective Prandtl number formulation of Ahluwalia and Doss [13].

Complete numerical solution

The finite-differencing method used to solve numerically the gasdynamic equations is essentially that described in [9] and, therefore its details are not repeated here. The new feature is the inclusion of radiation terms in the energy equation. These terms are treated as source terms, i.e. they are evaluated for a temperature distribution prevailing at the immediately preceding upstream station. Spectral integration involved in equation (7) is made accurate by dividing the large integration domain ($200–15\,000\ cm^{-1}$) into 7 bands. Integration over these bands is performed by adopting a 16-point Gaussian quadrature scheme. As indicated in [2], radiation terms are not updated at each marching step, nor are they calculated at all grid points at any step. Had these modifications not been adopted, the computational time would have been on the order of 20 h CPU time, as opposed to 15 CPU min now typically required. Numerical computations were performed on IBM 370/195 and 3033 machines.

RESULTS AND DISCUSSION

The computed exit conditions of [2] for a channel with rough walls are taken as the natural entrance conditions for the diffuser; these are: pressure = 0.85 atm, centerline temperature = 2350 K, and boundary layer thickness = 0.51 m.The mass flow rate through the diffuser is 350 kg s^{-1} and the total thermal input to the diffuser is 1250 MW. The diffuser is selected to be 15 m in length and, to be compatible with the channel of [2], measures 2 × 2 m at inlet. The diffuser walls diverge equally in electrode and sidewall directions and are considered to be moderately rough, of 3 mm roughness; as is characteristic of slag-coated walls, a slag surface temperature of 1800 K is assumed. The base calculations are performed for Rosebud coal ash, wall emissivity of 0.8 and diffuser divergence half-angle of 1.43°. Sensitivity of the results to changes from base conditions is assessed by studying the diffuser behavior for Centralia power plant coal ash, for wall emissivity of 0.5, and for diffuser divergence half-angles of 1.0, 2.0, 2.5, and 3.0 degrees.

To be consistent with the channel calculations thermodynamic properties corresponding to equilib-

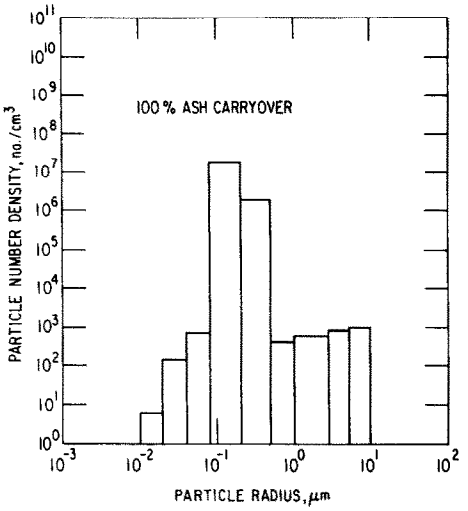

FIG. 1. Histogram for 100% ash carryover.

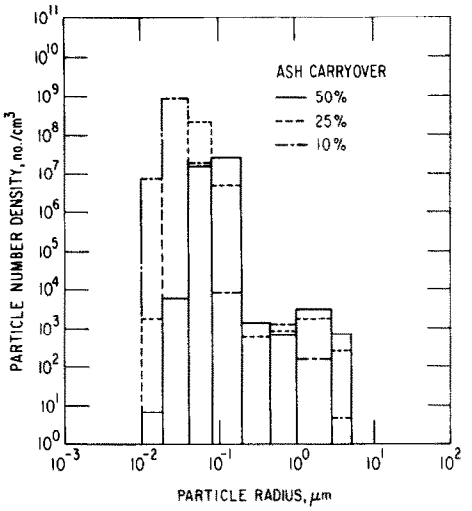

FIG. 2. Histogram for 10, 25, and 50% ash carryover.

rium combustion of 5% moist coal with preheated, oxygen-vitiated air are used. Thermodynamic data showed that in the pressure and temperature range of interest, mole fractions of CO_2, H_2O, and K could be taken as 0.20, 0.12 and 0.004 in that order [2].

Histograms

As pointed out in the Introduction, slag particles play a dominant role in promoting radiative heat transfer in the diffuser. These slag particles originate mostly from the ash vaporized in the combustor and subsequently nucleated in the channel. Some of the unvaporized slag particles also flow into the channel. Im and Ahluwalia [2] have shown that the slag particles are not mono-sized but have a characteristic bi-modal spectrum. This particle size spectrum was found to depend intimately upon the channel operating conditions, ash carryover rate, and liquid droplet-to-slag vapor ratio at channel inlet. The last two parameters are principally functions of combustor flow configuration. An objective of the present task is to study the diffuser performance for the various spectra of particle sizes at channel exit that were presented in [2].

It is important to recognize that the complete particle spectrum must be considered in computing the radiative heat transfer by slag particles. To emphasize this point, reference is made to equations (22) and (23), which indicate the efficiency factors for extinction and scattering to be functions of two parameters, namely, the complex refractive index and the nondimensional group, $2\pi r/\lambda$. Equations (24) and (25) further emphasize the dependence of the extinction coefficient and scattering albedo on the particle distribution function. Intuitively, small particles ($2\pi r/\lambda \ll 1$) absorb more radiation than they scatter, intermediate-size particles ($2\pi r/\lambda \simeq 1$) absorb and scatter radiation in comparable amounts, and particles of large size ($2\pi r/\lambda \gg 1$) are more effective in scattering radiation. Mie theory confirms the validity of this intuition. It is worth mentioning that a sample calculation of [14] proved that a cloud of gas containing mono-dispersed particles has lower emissivity than if it had distributed-size particles of the same total number density and the same average size. With this background, we seek an accurate representation of particle spectra presented in [2]. A simple and accurate representation is in the form of a histogram.

Figure 1 is a nine-band histogram representative of the particle size spectrum for 100% ash carryover into the channel. Figure 2 is an eight-band histogram for the situation in which the amount of ash vaporizing in combustor is less than the maximum possible. Im and Ahluwalia [2] should be consulted for detailed explanations concerning the spectra itself. In analogy to the concept of average size of a distribution function, the ordinates of these histograms were determined from the following equation

$$\bar{N}_i = \frac{\Sigma N_j r_j}{\bar{r}_i} \tag{33}$$

where i refers to a band, $\bar{r}_i$ is the median size of the band, and the summation is performed for all the particles lying within the band; $\bar{N}_i$s calculated from (33) were used in determining β_ν and ω_ν in equations (24) and (25).

Effect of slag carryover

Figure 3 shows the variation of radiative and convective heat flux along the diffuser length for particle spectra corresponding to the histograms of Fig. 2. It is seen that whereas the convective heat flux decreases along the flow direction, the radiative heat flux does not. The axial drop in convective heat flux is attributed to boundary layer growth. The increase in the radiative heat flux along the axial direction is partly credited to divergent diffuser geometry, which leads to higher optical thickness downstream. More

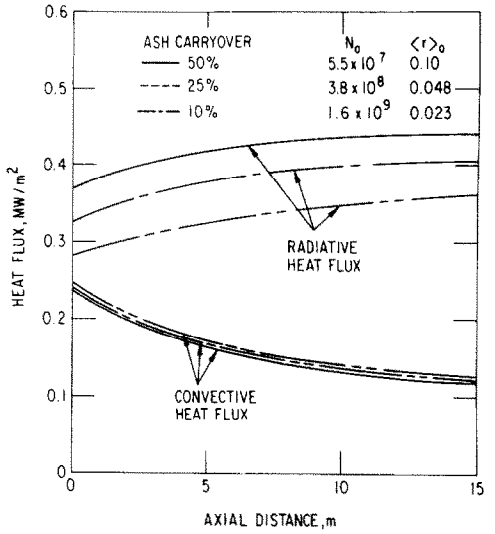

FIG. 3. Heat flux characteristics for different ash carryover rates.

importantly, as flow Mach number decreases, a conversion of kinetic energy to thermal energy takes place. This conversion of energy more than compensates for the diffuser heat loss in the form of convection and radiation. Consequently, the centerline temperature, and the average temperature as well, increase along the flow direction. This temperature rise is mainly responsible for increasing radiative heat flux along the flow direction. This is one distinguishing feature of the nature of radiative heat transfer from the slag particle-laden gas in the MHD diffuser. For a black body, the radiation heat flux is proportional to the fourth power of temperature. For a real gas, however, the gas emissivity decreases with temperature so that the dependence of gas radiation on temperature is less than the fourth power. For a slag particle-laden gas, the medium emissivity may increase with temperature for the reason that the electrical conductivity of slag particles, a parameter that determines the absorption coefficient, is exponentially dependent upon gas temperature. Therefore, depending on electrical conductivity variation and size and number density of particles, the exponent of temperature for proportionality between radiation of a gas medium containing slag particles and temperature may be greater than four. Another reason that contributes to enhancement of gas emissivity with temperature is the presence of potassium atoms which absorb thermal radiation of short wavelengths around 0.78 μm. As the gas temperature is raised, the peak of the black body intensity shifts toward the shorter wavelength region; this follows from the Wien's displacement law. As a result, with increase of gas temperature, the potassium atoms become more active in absorbing and hence attenuating the thermal radiation so that the gas emissivity rises with temperature.

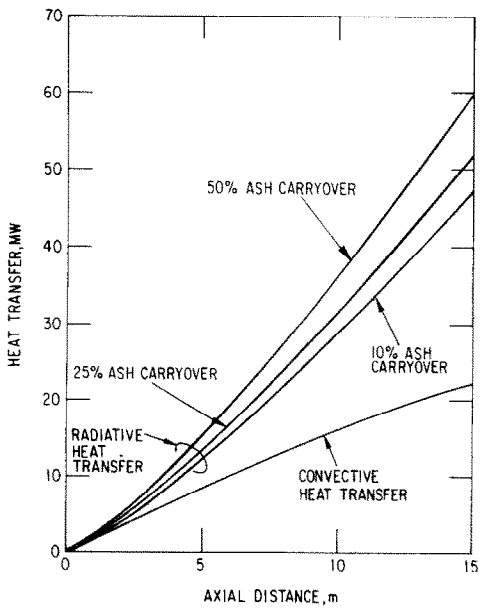

FIG. 4. Heat transfer characteristics.

Figure 3 shows that radiative heat flux increases with the ash carryover rate into the channel. There are two reasons for this. First, with a higher ash carryover rate, in spite of lower number density, the particles have a greater collective surface area ($\equiv \Sigma \bar{N}_i r_i^2$), and this leads to a higher absorption coefficient. Secondly, as the ash carryover rate becomes higher, the number of particles in the larger size range increases (see Fig. 2). As mentioned earlier, larger particles ($2\pi r/\lambda \gg 1$) scatter more radiation than they absorb, thus providing the smaller particles, which are effective absorbers, with an additional opportunity to absorb the scattered radiation. This process becomes more effective with the possibility of multiple scattering.

The importance of radiation in Fig. 3 is very pronounced. Radiative heat flux exceeds the convective flux by a factor as high as four. The contribution of radiation can be directly ascertained from Fig. 4. The heat transfer by convection is nearly 25 MW; the radiative heat transfer varies from 44 MW for the case of 10% ash carryover from the combustor to 62 MW for the 50% case. For 100% ash carryover, the heat transfer by radiation is 79 MW (see Fig. 5). For all cases considered, the total heat transfer lies between 70 and 100 MW.

Nature of radiation

To identify the critical parameters that control heat transfer in the diffuser, results are given in Figs. 6, 7, and 8 by changing one or more conditions of the reference case. Curve A of Fig. 6 represents the base case. Note that radiative flux first increases in the axial direction and then decreases. At the front end of the diffuser, the total heat transfer is small enough (because of small specific volume of the diffuser) that the conversion of kinetic to thermal energy can compensate for the heat loss, so that there is a rise in temperature. Consequently, the radiative heat flux

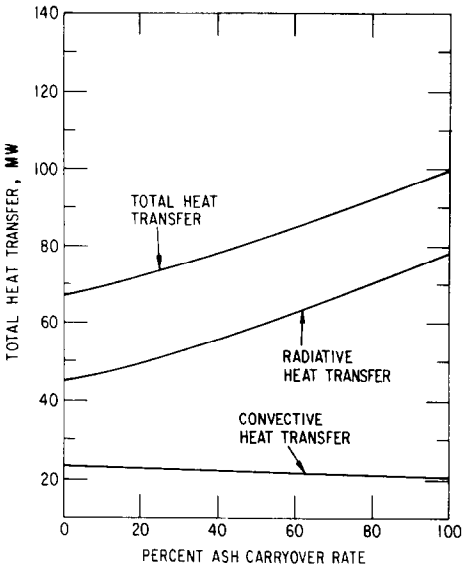

FIG. 5. Relationship between heat transfer and ash carryover rate.

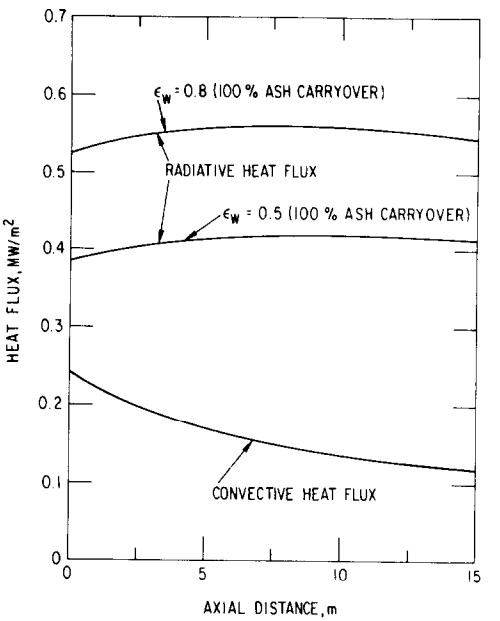

FIG. 7. Effect of wall emissivity on heat flux.

increases in magnitude. At the back end of the diffuser, the specific volume of the diffuser is large because of the divergent geometry so that the heat transfer rate is high even though the heat flux may be small. Also, the gas velocity has slowed down to the extent that the kinetic energy is only a small fraction of the thermal energy. Consequently, the conversion of kinetic to thermal energy cannot offset the heat loss and the gas temperature decreases. As a result, the radiative heat flux begins to decrease in spite of the higher optical thickness at the back end.

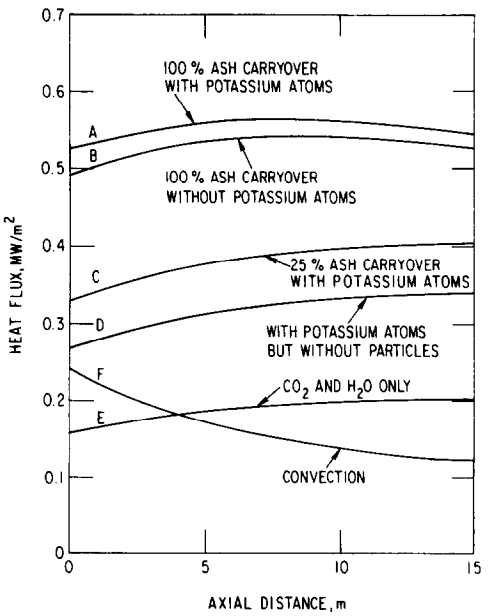

FIG. 6. Sensitivity of results.

Curve B is for a hypothetical situation in which no potassium atoms are present. Curve C is for 25% ash carryover. In Curve D, no particles are present; this would happen, for example, in a gas- or oil-fired MHD plant, except that mole fraction of water vapor would be much higher. Curve E represents the hypothetical situation in which neither particles nor potassium atoms are present. Curve F represents the contribution of convection.

The difference between curves A and C is attributed to the different particle spectra that emerge from change in the rate of ash carryover into the channel. The difference between curves A and D is a measure of the important role of the slag particles in promoting radiation. It is seen that the particle contribution is nearly 30–50% of the total radiative heat transfer. The difference between curves A and B measures the contribution of potassium atoms for the gas-plus-particles case, and between D and E indicates the contribution of K for the gas-only case. The differences between A and B and between D and E are not the same, thus proving the non-additive nature of contributions by individual participating species. It is interesting to note that particles tend to scatter the short wavelength radiation emitted by potassium. The disparity between the difference of curves A and B and of curves D and E is a measure of the radiation shielding effect of the particles by multiple scattering.

Figure 7 shows the influence of wall emissivity on radiation heat transfer. A 30% reduction of heat flux is observed when the wall emissivity is lowered to 0.5 from 0.8. A wall emissivity of 0.5 is believed to be the lower limit.

Figure 8 shows the effect of electrical conductivity of particles on radiative heat transfer. The electrical conductivity data of [1] and [15] have been curve-fitted for $T > 1600$ K by the following correlations

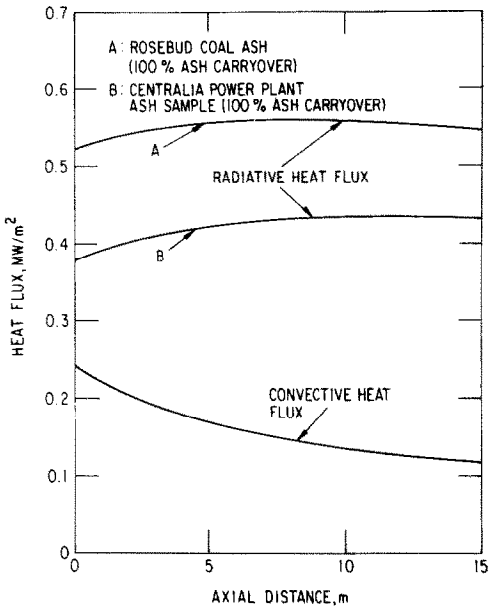

FIG. 8. Effect of electrical conductivity on heat flux.

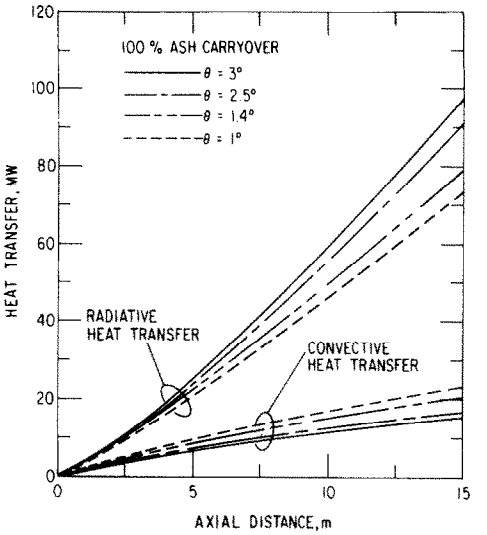

FIG. 9. Diffuser performance.

Rosebud coal: $\sigma_e = 10 \exp(12.65 - 2.3 \times 10^4/T)$

Centralia: $\sigma_e = 0.5 \exp(13.5 - 2.08 \times 10^4/T)$.

Electrical conductivity enters the calculations through complex refractive index ($m = 1.5 - i30\lambda\sigma_e$). The higher the electrical conductivity of slag particles, the greater is the efficiency factor for extinction. Figure 8 indicates a 30% difference in radiation heat fluxes for Rosebud coal ash, considered to be of medium electrical conductivity, and Centralia power plant coal ash [1], considered to be of low electrical conductivity.

Diffuser performance

Figure 9 presents the influence of diffuser half-divergence angle on heat transfer. As the divergence angle is increased, the specific volume increases faster with distance so that the radiative heat flux increases also. The lowering of convective heat flux with divergence angle is indicative of a faster rate of boundary layer growth. In Table 1, the average velocity and blockage at diffuser exit, (defined as $(1 - 2\delta_{1s}/W)^2$ for square cross-sections) and the corresponding pressure recovery coefficient, are listed. For 3° divergence angle, the flow may separate anywhere beyond $x = 10$ m. For all four cases, the average exit temperature was ~2300 K. For 2.5° and 3.0° divergence angles, the flow became fully developed before reaching the exit.

CONCLUSIONS

A quasi-three-dimensional diffuser model has been formulated and solved by a coupled analytical and numerical technique. The radiative contributions of carbon dioxide, water vapor, and potassium atoms are all included. The formulation also incorporates the role of slag particles in absorbing and scattering radiation. The important conclusions drawn from the results of the analysis are listed below.

(1) Although the convective heat flux in the diffuser decreases along the axial direction (because of boundary layer growth), the radiative heat flux may increase in that direction because of diffuser divergence and the possible rise in gas temperature resulting from the conversion of kinetic to thermal energy. For the base conditions of a 1700 MW thermal MHD plant, the total convective heat transfer in the diffuser is 25 MW, and the radiative heat transfer lies between 44 MW for 8% ash carryover and 79 MW for 100% ash carryover into the channel. This shows the importance of accounting for radiation in diffuser heat transfer computations.

(2) The results demonstrate that slag particles play

Table 1. Diffuser performance

θ	Area ratio	$\langle u \rangle$ (m s^{-1})	Blockage	C_p	Comment
1.0	1.58	453	0.45	0.33	No boundary layer separation
1.4	1.87	406	0.54	0.39	No boundary layer separation
2.5	2.71	317	0.66	0.46	Fully developed flow
3.0	3.17	283	0.69	0.48	Separation tendency

a dominant role in promoting radiant heat transfer. It was inferred that the radiative flux resulting from particles is more than twice that resulting from carbon dioxide and water vapor. Moreover, the phenomenon of particles shielding radiation through multiple scattering was identified. This shielding effect is a manifestation of the particles scattering the short wavelength radiation that is emitted by potassium.

(3) The sensitivity of results to changes from reference conditions was established. It was observed that changing the wall emissivity from 0.8 to 0.5, or changing the electrical conductivity, modifies the radiative flux by 30%. The influence of diffuser half-divergence angle on heat transfer has been discussed. In view of the importance of radiation, a systematic study of the influence of diffuser inlet conditions on diffuser performance, as studied in [4] with radiation omitted, needs further elaboration.

Acknowledgement—This research was sponsored by U.S. Department of Energy, MHD Division.

REFERENCES

1. M. Petrick and B. Y. Shumyasky, *Open-Cycle Magnetohydrodynamic Electrical Power Generation*, pp. 559–568 and 622–676. A Joint U.S.A./U.S.S.R. Publication, Argonne National Laboratory, Argonne (1978).
2. K. H. Im and R. K. Ahluwalia. Heat and mass transfer in MHD channels, *J. Energy*, **5**, 22–30 (1981).
3. K. H. Im and P. M. Chung, Nucleation and evolution of slag droplets in coal combustion, *A.I.Ch.E. Jl* **26**, 655–664 (1980).
4. E. D. Doss, Subsonic MHD-diffuser performance with high blockage, *J. Energy* **1**, 370–375 (1977).
5. G. D. Roy, On supersonic and subsonic diffusers for magnetohydrodynamic generator applications, fluids engineering in advanced energy systems, *Conference Proceedings of the Winter Annual Meeting of ASME*, 139–152 (1978).
6. H. C. Van de Hulst, *Light Scattering by Small Particles*, pp. 119–128. John Wiley, New York (1957).
7. C. L. Tien, Thermal radiation properties of gases, *Adv. Heat Transfer* **5**, 253–324 (1968).
8. B. Davison and J. B. Sykes, *Neutron Transport Theory*, pp. 157–173, Chap. XII. Oxford University Press, London (1958).
9. R. K. Ahluwalia and E. D. Doss, Quasi-three-dimensional modeling of flow in MHD channels, *Numer. Heat Transfer* **3**, 67–87 (1980).
10. C. Mark, The spherical harmonic method I, National Research Council of Canada, Division of Atomic Energy, TM-92 (1944).
11. T. Cebeci and A. M. O. Smith, *Analysis of Turbulent Boundary Layers*, Chap. 6. Academic Press, New York (1974).
12. T. Cebeci and K. C. Chang, Calculations of rough-wall boundary-layer flow, *AIAA Jl* **16**, 993–1003 (1971).
13. R. K. Ahluwalia and E. D. Doss, Convective heat transfer in MHD channels and its influence on channel performance, *J. Energy* **4**, 126–134 (1980).
14. K. H. Im and T. R. Johnson, Effective emissivity and absorptivity of combustion gas with slag particles, Argonne National Laboratory, Argonne, ANL/MHD-79-14 (to be published).
15. R. Pallina and R. Larsen, MHD slag conductivity studies, *17th Symposium on Engineering Aspects of MHD*, Stanford, C.6.1-C.6.6 (1978).

COMBINAISON DE LA CONDUCTION DE LA CONVECTION DU RAYONNEMENT DES GAZ ET DES PARTICULES DANS LES DIFFUSEURS MHD

Résumé — Le transfert thermique dans les diffuseurs MHD par conduction, convection, rayonnement du gaz et des particules est analysé en résolvant simultanément l'équation du transfert par rayonnement et les équations de la dynamique des gaz. On considère que le gaz carbonique, la vapeur d'eau et les atomes de potassium sont les principaux gaz qui participent au rayonnement. L'équation de transfert du rayonnement non-gris est résolue en s'appuyant sur l'approximation P_1. Les coefficients d'absorption de CO_2 et H_2O sont évalués par le modèle exponentiel à large bande et celui des atomes K par certaines formulations. Les facteurs d'efficacité pour l'extinction et la diffusion par les particules sont calculés à partir de la théorie de Mie. En référence à une géométrie de diffuseur appropriée à une unité MHD de 1700 MW thermique, le transfert de chaleur par convection est de 25 MW et celui par rayonnement varie de 44 MW à 79 MW suivant la concentration de cendre emportée dans le canal. Les résultats montrent que le résultat est sensible à la poussière, au spectre de dimension des particules, à sa conductivité électrique à la composition des gaz et à l'émissivité de la paroi. On observe qu'à cause de la diffusion multiple, les particules masquent le rayonnement des atomes de potassium émis dans les courtes longueurs d'onde.

DAS ZUSAMMENWIRKEN VON LEITUNG, KONVEKTION UND STRAHLUNG VON GAS SOWIE FESTSTOFFEN IN MHD-DIFFUSOREN

Zusammenfassung—Der Wärmeübergang in MHD-Diffusoren durch Leitung, Konvektion und Strahlung von Gas und Schlackepartikeln wird durch simultane Lösung der Strahlungstransport-Gleichung und eines Satzes von quasi-dreidimensionalen gasdynamischen Gleichungen untersucht. Kohlendioxid, Wasserdampf und Kalium-Atome werden als die wesentlichen Gase betrachtet, die an der Gasstrahlung beteiligt sind. Die Strahlungstransportgleichung für nicht-graue Strahler wird durch Anwenden der P_1-Approximation gelöst. Die Absorptionskoeffizienten für CO_2 und H_2O werden aus dem exponentiellen Breitband-Modell, die für K-Atome aus gewissen Korrelationen abgeschätzt. Die Faktoren der Extinktion und der Streuung von Partikeln werden nach der Mie-Theorie berechnet. Für eine Diffusorgeometrie, die einem 1700 MW MHD-Wärmekraftwerk entspricht, wurde der Wärmeübergang durch Konvektion zu 25 MW berechnet, während der Wärmeübergang durch Strahlung im Bereich von 44 MW bis 79 MW liegt, je nachdem, wieviel Asche in den Kanal gelangt. Die Ergebnisse zeigen, daß der Wärmeübergang vom Aschegehalt der Strömung, vom Größenspektrum der Schlackepartikel, von der elektrischen Leitfähigkeit der Asche, der Gaszusammensetzung und dem Emissionsvermögen der Wand abhängt. Es wurde beobachtet, daß die Partikel die kurzwellige Strahlung der Kalium-Atome durch Mehrfachstreuung abschirmen.

ВЗАИМОСВЯЗАННЫЕ ПРОЦЕССЫ ТЕПЛОПРОВОДНОСТИ, КОНВЕКЦИИ И ИЗЛУЧЕНИЯ ГАЗА И ЧАСТИЦ В МГД ДИФФУЗОРАХ

Аннотация — Передача тепла теплопроводностью, конвекцией и излучением (как от газа, так и от частиц шкала) в МГД диффузорах анализируется путем совместного решения уравнения переноса излучения и системы квазитрехмерных газодинамических уравнений. В качестве основных газообразных компонентов, участвующих в процессе излучения, рассматриваются атомы двуокиси углерода, водяного пара и калия. Уравнение переноса несерого излучения решается с помощью P_1 — приближения. Коэффициенты поглощения для CO_2 и H_2O рассчитываются по экспоненциальной широкополосной модели, а для атомов К — из известных соотношений. Коэффициенты затухания и рассеяния излучения частицами рассчитываются по теории Ми. Найдено, что для диффузора эталонной геометрии, предназначенного для тепловой магнитогазодинамической установки на 1700 МВт, величина конвективного теплопереноса составляет 25 МВт, а лучистого изменяется от 44 МВт до 79 МВт в зависимости от интенсивности выноса золы. Результаты свидетельствуют о том, что теплообмен зависит от скорости уноса золы, распределения размеров частиц шлака, электропроводности золы, состава газа и степени черноты стенки. Показано, что многократное рассеяние, вызываемое частицами, экранирует коротковолновое излучение, испускаемое атомами калия.